

# An asymptotic-preserving IMEX method for nonlinear radiative transfer equation

Weiming Li<sup>\*</sup>, Peng Song<sup>†</sup>, Yanli Wang<sup>‡</sup>

September 15, 2020

## Abstract

We present an asymptotic preserving method for the radiative transfer equations in the framework of  $P_N$  method. An implicit and explicit method is proposed to solve the  $P_N$  system based on the order analysis of the expansion coefficients of the distribution function. The order of each coefficient expanded in the Knudsen number is found through the process of Maxwellian iteration, and the coefficients of high order are treated explicitly while that of low order are treated implicitly in each equation of  $P_N$  system. Energy inequality is proved for this numerical scheme. Several numerical examples validate this new AP scheme in both optical thick and thin regions.

**key word:** radiative transfer equations; asymptotic preserving; energy stability

## 1 Introduction

Radiation plays an important role in thermal radiative transfer in inertial confinement fusion. Thermal radiative transfer is an intrinsic component of coupled radiation-hydrodynamic problems [26]. The radiative transfer equations (RTE) are always adopted to describe the energy exchange between different materials in the system. However, this system is of high dimensionality. Precisely, the independent variables are position, angle, frequency and time, which depend on a seven-dimensional phase space and lead to expensive computational complicity [17]. Moreover, the radiation travels at the speed of light and has very restrictive limit on the time-step size for the time-explicit schemes, or the implicit schemes are required. Therefore, solving the RTE system numerically is a challenging problem [39].

Generally speaking, there are two kinds of methods to solve this system, the stochastic and deterministic methods. The stochastic methods, generate random numbers to simulate the discrete interactions of individual radiation particle with the background material. There is no ray effect in the stochastic method but it suffers from the statistical noise [6]. One of the popular stochastic methods is the implicit Monte Carlo (IMC) method [6]. The IMC method has shown to be efficient in optically thin regions. However, it needs quite large amount of particles in the optically thick regions, which make IMC inefficient. Several efforts have been made to improve the efficiency of IMC method, such as [7, 3, 4, 34], which we will not discuss in detail here. Recently, series of unified gas-kinetic schemes (unified gas-kinetic particle method (UGKP) [23, 38] and unified gas-kinetic wave particle method (UGKWP) [24]) are proposed to solve RTE system, where a particle-based Monte Carlo solver is proposed to track the non-equilibrium transport. For the deterministic methods, the discrete-ordinates ( $S_N$ ) method is often adopted [15, 21]. In this method, the transport equation is solved along particular directions and the energy density is reconstructed using a quadrature rule.  $S_N$  method has been studied for many years and several efforts have been made to improve the efficiency of this method [41]. However,  $S_N$  methods suffer from ray-effects [32, 25], which will lead to hot spot in the material, thus the material will consequently evolve incorrectly.

Another deterministic method is the spherical harmonics ( $P_N$ ) method [13, 22]. In the framework of  $P_N$  method, the radiation intensity is approximated by a series expansion of polynomials in the angular space.  $P_N$  method does not have ray effects in multiple dimensional cases in the spatial space. However,

<sup>\*</sup>Laboratory of Computational Physics, Institute of Applied Physics and Computational Mathematics, Beijing, China, 100088, email: [liweiming@pku.edu.cn](mailto:liweiming@pku.edu.cn)

<sup>†</sup>Laboratory of Computational Physics, Institute of Applied Physics and Computational Mathematics, Beijing, China, 100088, email: [song-peng@iapcm.ac.cn](mailto:song-peng@iapcm.ac.cn)

<sup>‡</sup>Beijing Computational Science Research Center, Beijing, China, 100193, email: [ylwang@csrcc.ac.cn](mailto:ylwang@csrcc.ac.cn).

the spatially and temporally continuous  $P_N$  method may lead to negative energy density solution, which limits the usage of  $P_N$  method [28]. Several attempts are made to correct the negativity in  $P_N$  equations, such as the filtered  $P_N$  method which is proposed to solve this problem [27, 17] and adding artificial scattering terms [33]. However,  $P_N$  method may generally has to be implemented with an implicit time-integration scheme, due to the extremely fast transport velocity. Moreover, in the optical thick regime, the photon's mean-free path is quite small. Thus, the spatial mesh size, which should be comparable to the photon's mean-free path, is also very small and will lead to very expensive computational cost [39].

The asymptotic preserving (AP) scheme for the kinetic equation is proposed to solve this problem [10, 11, 12]. AP scheme has been studied in several literature [39, 40, 14]. An AP scheme will recover the diffusion solution automatically with the Knudsen number going to zero, when holding the time step and mesh size fixed [14, 18, 19, 31]. We in this paper, will develop such an AP scheme for the gray radiation transfer equations in the framework of  $P_N$  method. The radiation intensity is first approximated by series expansion of polynomials. Then the Maxwell iteration method is utilized to get the order of the expansion coefficients referred to Knudsen number, based on which an implicit-explicit scheme is designed for  $P_N$  system. In this scheme, the term at higher order of Knudsen number is solved explicitly with those at lower order solved implicitly in each equation of  $P_N$  system. In this case, the implicit-explicit  $P_N$  system is changed into a pseudo implicit system, which could be solved at the computational cost of an explicit scheme. Moreover, the energy exchange term is solved implicitly, which will greatly release the restriction on the time step length. The equation for the material energy is solved coupled with  $P_N$  system, which is reduced into a fourth degree polynomial equation.

For cases with solutions of spatial variation in two-dimensions, when the Knudsen number goes to zero, the resulting  $P_N$  system is reduced into a five points diffusion scheme for the material temperature. Numerical examples is tested first to validate the AP property of this numerical scheme, which is also extended to the high order IMEX RK scheme. We have analyzed the variation of the total energy, and prove the energy inequality with the evolution of time. The classical Marshak wave problems in 1D spatial space and the lattice problem and the hohlraum problem in 2D spatial space are tested to verify the effectiveness of this numerical scheme.

The rest of this paper is organized as follows: Section 2 will introduce the RTE system and  $P_N$  method. The AP IMEX method is presented and discussed in detail in Section 3, with the AP property and energy stability proved in Section 4. Several numerical examples will be exhibited in Section 5. The conclusion and future work will be stated in Section 6.  $P_N$  system for 1D RTE system and the boundary conditions are discussed in Appendix A.

## 2 Radiative transfer equations and $P_N$ method

In the absence of hydrodynamic motion and heat conduction, the radiative transfer equations (RTE) is composed with the transfer equations of the radiation intensity and the associated energy balance equations. In this section, we will introduce the gray radiative transfer equations. The  $P_N$  method, which is one of the most popular numerical methods to solve RTE, will also be presented.

### 2.1 System of the gray radiative transfer equations

The radiative transfer and the energy exchange between radiation and material are described by the gray radiative transfer equations, which has the form below:

$$\frac{\epsilon^2}{c} \frac{\partial I}{\partial t} + \epsilon \mathbf{\Omega} \cdot \nabla I = \sigma \left( \frac{1}{4\pi} acT^4 - I \right), \quad (2.1a)$$

$$\epsilon^2 C_v \frac{\partial T}{\partial t} \equiv \epsilon^2 \frac{\partial U}{\partial t} = \sigma \left( \int_{\mathbb{S}^2} I d\mathbf{\Omega} - acT^4 \right). \quad (2.1b)$$

Here  $\mathbf{\Omega}$  is the angular variable which lies on  $\mathbb{S}^2$ , the surface of the unit sphere. Also,  $I(\mathbf{x}, t, \mathbf{\Omega})$  is the radiation intensity,  $\mathbf{x}$  is the spatial variable, and  $\sigma(\mathbf{x}, T)$  is the opacity. In (2.1), the external source and scattering terms are omitted.  $T(\mathbf{x}, t)$  is the material temperature and  $c$  is the speed of light. The relationship between the material temperature  $T(\mathbf{x}, t)$  and the material energy density  $U(\mathbf{x}, t)$  is

$$\frac{\partial U}{\partial T} = C_v > 0, \quad (2.2)$$

where  $C_v(\mathbf{x}, t)$  is the heat capacity. Integrating (2.1a) with  $\mathbf{\Omega}$ , and adding (2.1b), we can get the conservation of energy

$$\epsilon^2 C_v \frac{\partial T}{\partial t} + \epsilon^2 \frac{\partial E}{\partial t} + \epsilon \int_{\mathbb{S}^2} \mathbf{\Omega} \cdot \nabla I \, d\mathbf{\Omega} = 0, \quad (2.3)$$

where  $E$  is the energy density defined as

$$E = \frac{1}{c} \int_{\mathbb{S}^2} I \, d\mathbf{\Omega}. \quad (2.4)$$

The total energy is then defined as

$$\mathcal{E} = U + E. \quad (2.5)$$

The parameter  $\epsilon$  in (2.1) is the Knudsen number. When  $\epsilon$  goes to zero, the intensity  $I$  goes to a Planckian at the local temperature [40, 39], and the corresponding local temperature  $T^{(0)}$  satisfies the nonlinear limited diffusion equation

$$\frac{\partial U(T^{(0)})}{\partial t} + a \frac{\partial}{\partial t} \left( T^{(0)} \right)^4 = \nabla \cdot \frac{ac}{3\sigma} \nabla \left( T^{(0)} \right)^4, \quad I^{(0)} = ac \left( T^{(0)} \right)^4, \quad (2.6)$$

where  $a$  is the radiation constant given by

$$a = \frac{8\pi k^4}{15h^3 c^3}, \quad (2.7)$$

and  $h$  is Planck's constant while  $k$  is Boltzmann constant. In this approximation, the radiative flux  $F(t, \mathbf{x})$  is related to the material temperature by a Fick's law of diffusion given by

$$\int_{\mathbb{S}^2} \mathbf{\Omega} I \, d\mathbf{\Omega} = F(t, \mathbf{x}) = -\frac{ac}{3\sigma} \nabla T^4. \quad (2.8)$$

Moreover, at this time the total energy (2.5) is expressed as

$$\mathcal{E} = U^{(0)} + a \left( T^{(0)} \right)^4. \quad (2.9)$$

Direct simulation of the radiative transfer equations (2.1) is costly for several reasons. First, the independent variables of (2.1) are position, angle, and time, therefore usually seven-dimensional, making it expensive to simulate. Then, the radiation travels at the speed of light, therefore, the corresponding CFL limit on time-step length for time-explicit schemes is quite restrictive. Finally, when the Knudsen number is small, (2.1) contain stiff source terms, leading to stringent restrictions on the time step for time-explicit schemes. On the other hand, (2.1) go to the diffusion limit (2.6) as the Knudsen number approaches zero, so a popular approach to solve this problem is to construct the asymptotic-preserving (AP) schemes for the kinetic equations [12, 11].

In this paper, we will propose an AP IMEX(IMPlicit-EXplicit) scheme under the framework of the  $P_N$  method to numerically solve (2.1). In the next section, we will first introduce  $P_N$  method to solve (2.1).

## 2.2 $P_N$ system

The  $P_N$  method approximates the angular dependence of (2.1) by a series expansion of the spherical harmonics function. The moments of the intensity is defined as

$$I_l^m(\mathbf{x}, t) = 2\sqrt{\pi} \int_{\mathbb{S}^2} \bar{Y}_l^m(\mathbf{\Omega}) I(\mathbf{x}, t, \mathbf{\Omega}) \, d\mathbf{\Omega}, \quad (2.10)$$

where  $Y_l^m(\mathbf{\Omega})$  is the spherical harmonics

$$Y_l^m(\mathbf{\Omega}) = \sqrt{\frac{2l+1}{4\pi} \frac{(l-m)!}{(l+m)!}} P_l^m(\cos \theta) \exp(im\phi), \quad \mathbf{\Omega} = (\sin \theta \cos \phi, \sin \theta \sin \phi, \cos \theta)^T, \quad (2.11)$$

with  $P_l^m(x)$  an associated Legendre polynomial. Then multiplying (2.1a) on both sides by  $\bar{Y}_l^m(\mathbf{\Omega})$  and integrating against  $\mathbf{\Omega}$ , we can derive the detailed form of the  $P_N$  equations for (2.1a) [29] as

$$\begin{aligned} \frac{\epsilon^2}{c} \frac{\partial I_l^m}{\partial t} + \frac{\epsilon}{2} \frac{\partial}{\partial x} \left( -C_{l-1}^{m-1} I_{l-1}^{m-1} + D_{l+1}^{m-1} I_{l+1}^{m-1} + \mathcal{E}_{l-1}^{m+1} I_{l-1}^{m+1} - F_{l+1}^{m+1} I_{l+1}^{m+1} \right) \\ + \epsilon \frac{\partial}{\partial z} \left( A_{l-1}^m I_{l-1}^m + B_{l+1}^m I_{l+1}^m \right) = -\sigma I_l^m + \sigma ac T^4 \delta_{l0} \delta_{m0}, \quad l \in \mathbb{N}, \quad m \in \mathbb{Z}, \quad |m| \leq l, \end{aligned} \quad (2.12)$$

where  $\delta_{ij}$  is the Kronecker-delta function, and the coefficients are

$$\begin{aligned} A_l^m &= \sqrt{\frac{(l-m+1)(l+m+1)}{(2l+3)(2l+1)}}, & B_l^m &= \sqrt{\frac{(l-m)(l+m)}{(2l+1)(2l-1)}}, \\ C_l^m &= \sqrt{\frac{(l+m+1)(l+m+2)}{(2l+3)(2l+1)}}, & D_l^m &= \sqrt{\frac{(l-m)(l-m-1)}{(2l+1)(2l-1)}}, \\ \mathcal{E}_l^m &= \sqrt{\frac{(l-m+1)(l-m+2)}{(2l+3)(2l+1)}}, & F_l^m &= \sqrt{\frac{(l+m)(l+m-1)}{(2l+1)(2l-1)}}. \end{aligned} \quad (2.13)$$

The derivation of the moment system (2.12) is discussed in several literature, and we refer to [37, 29] for more details. Especially, the governing equations for the zeroth moment  $I_0^0$  is

$$\frac{\epsilon^2}{c} \frac{\partial I_0^0}{\partial t} + \frac{\epsilon}{2} \frac{\partial}{\partial x} (D_1^{-1} I_1^{-1} - F_1^1 I_1^1) + \epsilon \frac{\partial}{\partial z} B_1^0 I_1^0 = -\sigma I_0^0 + \sigma ac T^4, \quad (2.14a)$$

and the zeroth moment of the intensity with the energy density is

$$E = \frac{1}{c} \int_{\mathbb{S}^2} I(t, \mathbf{x}, \boldsymbol{\Omega}) d\boldsymbol{\Omega} = \frac{I_0^0}{c}. \quad (2.15)$$

In the framework of  $P_N$  method, the governing equations of the total energy (2.3) is

$$C_v \frac{\partial T}{\partial t} + \frac{1}{c} \frac{\partial I_0^0}{\partial t} + \frac{1}{\epsilon} \left( \frac{1}{2} \frac{\partial}{\partial x} (D_1^{-1} I_1^{-1} - F_1^1 I_1^1) + \frac{\partial}{\partial z} B_1^0 I_1^0 \right) = 0. \quad (2.16)$$

Gathering (2.12) and (2.16), we get the governing equations for  $P_N$  system. The  $P_N$  equations will reduce the computational complexity to simulate (2.1). It is widely used to solve RTE, such as in [26, 31, 37]. However, the time step limitation and the multi-scale problem brought by Knudsen number still exist for  $P_N$  equations. In the next sections, we will propose an AP scheme for the  $P_N$  equations to release the restriction on the time step length.

### 3 Asymptotic-preserving IMEX method

In this section, we will introduce an asymptotic-preserving IMEX numerical scheme to solve (2.12) and (2.16). We will begin from the order analysis of the expansion coefficients referred to Knudsen number, based on which we will propose our new numerical scheme.

#### 3.1 Formal order analysis

In this section, we analyze the order of the expansion coefficients  $I_l^m$  based on  $\epsilon$ . We utilize the same technique of Maxwellian iteration as used for the Boltzmann equation in [2]. In order to get the order of  $I_l^m$ , we rewrite the governing equation (2.12) into

$$\frac{\epsilon^2}{c} \frac{\partial I_l^m}{\partial t} + \epsilon \nabla_{\mathbf{x}} F(I_{l-1}^m) + \epsilon \nabla_{\mathbf{x}} G(I_{l+1}^m) = -\sigma I_l^m, \quad l > 0, \quad m \in \mathbb{Z}, \quad |m| \leq l, \quad (3.1)$$

where

$$\begin{aligned} \nabla_{\mathbf{x}} F(I_{l-1}^m) &= \frac{\partial}{\partial x} \left( -C_{l-1}^{m-1} I_{l-1}^{m-1} + \mathcal{E}_{l-1}^{m+1} I_{l-1}^{m+1} \right) + \frac{\partial}{\partial z} A_{l-1}^m I_{l-1}^m, \\ \nabla_{\mathbf{x}} G(I_{l+1}^m) &= \frac{\partial}{\partial x} \left( D_{l+1}^{m-1} I_{l+1}^{m-1} - F_{l+1}^{m+1} I_{l+1}^{m+1} \right) + \frac{\partial}{\partial z} B_{l+1}^m I_{l+1}^m. \end{aligned} \quad (3.2)$$

Then we will begin Maxwellian iteration. We first rewrite (3.1) into an iterative scheme as

$$I_l^{m,(n+1)} = \epsilon \mathcal{J}_l^m \left( I_j^{k,(n)} \middle| l-1 \leq j \leq l+1, |k| \leq j \right) + \epsilon^2 \mathcal{H} \left( I_l^{m,(n)} \right), \quad l > 0, \quad m \in \mathbb{Z}, \quad |m| \leq l, \quad (3.3)$$

with the initial value  $I$  at equilibrium

$$I_0^{0,(0)} = acT^4, \quad I_l^{m,(0)} = 0, \quad \forall l \geq 1. \quad (3.4)$$

The first step of the iteration yields

$$\begin{aligned} I_1^{m,(1)} &= -\frac{\epsilon}{\sigma} \left( \frac{\partial}{2\partial x} \left( -C_0^{m-1} I_0^{m-1,(0)} + \mathcal{E}_0^{m+1} I_0^{m+1,(0)} \right) + \frac{\partial}{\partial z} A_0^m I_0^{m,(0)} \right), \quad |m| \leq 1, \\ I_l^{m,(1)} &= 0, \quad l > 1, \quad |m| \leq l. \end{aligned} \quad (3.5)$$

Assuming that the derivatives and  $\sigma$  are all at order  $\mathcal{O}(1)$ , it holds for  $I_1^m$  that

$$I_1^{m,(1)} = \mathcal{O}(\epsilon), \quad |m| \leq 1. \quad (3.6)$$

As  $\mathcal{J}_l^m$  and  $\mathcal{H}$  are both linear operators, only  $\mathcal{O}(\epsilon^2)$  terms are added in the second step of the iteration. Therefore, the leading order terms of  $I_1^m$  are

$$I_1^m \approx -\frac{\epsilon}{\sigma} \left( \frac{\partial}{2\partial x} \left( -C_0^{m-1} I_0^{m-1} + \mathcal{E}_0^{m+1} I_0^{m+1} \right) + \frac{\partial}{\partial z} A_0^m I_0^m \right) = \mathcal{O}(\epsilon), \quad |m| \leq 1. \quad (3.7)$$

By successively applying the iteration, we could deduce that the leading order of  $I_l^m$  is

$$I_l^m \approx -\frac{\epsilon}{\sigma} \nabla_{\mathbf{x}} F(I_{l-1}^m) = \mathcal{O}(\epsilon^l), \quad |m| \leq l. \quad (3.8)$$

For now, we have derived the order of the expansion coefficients based on  $\epsilon$ , based on which we will design the AP scheme.

*Remark 1.* (3.4) and (3.7) present the order of  $I_0^m$  and  $I_1^m$  respectively. Substituting both equations into the equation of total energy (2.16), we can get the same diffusion equation of  $T$  as (2.6) in the framework of  $P_N$  method with  $\epsilon$  going to zero.

### 3.2 Semi-discrete IMEX methods

For now, we have got the order of  $I_l^m$  based on  $\epsilon$ , based on which, we will introduce the semi-discrete scheme in time with globally stiffly accurate IMEX RK scheme. From the formal order analysis we find that in (3.1),

$$\epsilon \nabla_{\mathbf{x}} G(I_{l+1}^m) = \mathcal{O}(\epsilon^{l+2}), \quad \epsilon \nabla_{\mathbf{x}} F(I_{l-1}^m) = \mathcal{O}(\epsilon^l), \quad -\sigma I_l^m + \sigma acT^4 \delta_{l0} \delta_{m0} = \mathcal{O}(\epsilon^l). \quad (3.9)$$

The implicit-explicit strategy we adopt here is to treat all the terms with higher order of  $\epsilon$  explicitly with others implicitly. Thus in the numerical scheme, we set  $\nabla_{\mathbf{x}} G(I_{l+1}^m) = \mathcal{O}(\epsilon^{l+2})$  which is at higher order of  $\epsilon$  as the explicit term while  $\nabla_{\mathbf{x}} F(I_{l-1}^m)$  and the diffusion terms on the right side which are at lower order of  $\epsilon$  as the implicit term. Based on this, we will propose the first order semi-discretized scheme as

**First order scheme** Given  $(I_l^m)^n$ , and  $T^n$  to approximate the solution  $I_l^m$  and  $T$  at time  $n$ , the first order semi-discrete scheme to update the radiation density is

$$\frac{\epsilon^2}{c} \frac{(I_0^0)^{n+1} - (I_0^0)^n}{\Delta t} + \epsilon \left( \nabla_{\mathbf{x}} G(I_1^m) \right)^n = \sigma^n \left( ac(T^{n+1})^4 - (I_0^0)^{n+1} \right), \quad (3.10a)$$

$$C_v \frac{T^{n+1} - T^n}{\Delta t} + \frac{1}{c} \frac{(I_0^0)^{n+1} - (I_0^0)^n}{\Delta t} + \frac{1}{\epsilon} \left( \nabla_{\mathbf{x}} G(I_1^m) \right)^n = 0, \quad (3.10b)$$

$$\frac{\epsilon^2}{c} \frac{(I_l^m)^{n+1} - (I_l^m)^n}{\Delta t} + \epsilon \left( \nabla_{\mathbf{x}} F(I_{l-1}^m) \right)^{n+1} + \epsilon \left( \nabla_{\mathbf{x}} G(I_{l+1}^m) \right)^n = -\sigma^{n+1} (I_l^m)^{n+1}. \quad (3.10c)$$

Though the dominating terms in (3.10c) are treated implicitly, this first order numerical system (3.10) can actually be solved at the same computation cost as an explicit scheme. This is for the reason that when solving (3.10c), the terms with implicit scheme are already known.

In our implementation, we first solve the coupled system (3.10a) and (3.10b) to update  $(I_0^0)^{n+1}$  and  $T^{n+1}$ . Substituting (3.10a) into (3.10b) yields a fourth order polynomial equations of  $T^{n+1}$  as

$$C_v T^{n+1} + \frac{\Delta tac}{\epsilon^2 + \sigma^n \Delta tc} (T^{n+1})^4 - \left( C_v T^n + \frac{\sigma^n \Delta t}{\epsilon^2 + \sigma \Delta tc} (I_0^0)^n - \frac{\Delta t^2 c \sigma^n}{\epsilon(\epsilon^2 + \sigma^n \Delta tc)} \left( \nabla_{\mathbf{x}} G(I_1^m) \right)^n \right), \quad (3.11)$$

the solution of which will be guaranteed by the proposition below

**Proposition 1.** *The equation (3.11) has only one positive solution if positive solutions exist.*

The proof of proposition 1 is simple and will be omitted.

*Remark 2.* Though  $P_N$  is not a positive preserving method, for most of the problems we tested,  $I_0^0$  and  $T$  are kept positive in the computation. Positivity-preserving schemes for  $I_0^0$  and  $T$  will be the subject of future investigation.

This first order semi-discrete numerical scheme can be naturally extended to the high order IMEX RK scheme, which is listed as below

**High order IMEX RK scheme** To achieve higher order accuracy in time, we adopt the globally stiffly accurate IMEX RK scheme. The IMEX RK scheme is widely discussed [9, 42, 35], thus we only list the scheme here. The high order scheme is combined with the same implicit-explicit strategy as in the first order case. Precisely, the exact form is

$$\frac{\epsilon^2}{c}(I_0^0)^{n+1} = \frac{\epsilon^2}{c}(I_0^0)^n - \Delta t \sum_{k=1}^s \tilde{b}_k \epsilon \left( \nabla_{\mathbf{x}} G(I_1^m) \right)^k + \Delta t \sum_{k=1}^s b_k \sigma^{k-1} \left( ac(T^k)^4 - (I_0^0)^k \right), \quad (3.12a)$$

$$C_v \frac{T^{n+1} - T^n}{\Delta t} + \frac{1}{c} \frac{(I_0^0)^{n+1} - (I_0^0)^n}{\Delta t} + \frac{\Delta t}{\epsilon} \sum_{k=1}^s \tilde{b}_k \left( \nabla_{\mathbf{x}} G(I_1^m) \right)^k = 0, \quad (3.12b)$$

$$\frac{\epsilon^2}{c}(I_l^m)^{n+1} = \frac{\epsilon^2}{c}(I_l^m)^n - \Delta t \sum_{k=1}^s \tilde{b}_l \epsilon \left( \nabla_{\mathbf{x}} G(I_{l+1}^m) \right)^k - \Delta t \sum_{k=1}^s b_k \left( \left( \epsilon \nabla_{\mathbf{x}} F(I_{l-1}^m) \right)^k - \sigma^k (I_l^m)^k \right) = 0. \quad (3.12c)$$

where the approximations at the internal stages of an RK step satisfy

$$\frac{\epsilon^2}{c}(I_0^0)^k = \frac{\epsilon^2}{c}(I_0^0)^n - \Delta t \sum_{j=1}^{k-1} \tilde{a}_{kj} \epsilon \left( \nabla_{\mathbf{x}} G(I_1^m) \right)^j + \Delta t \sum_{j=1}^k a_{kj} \sigma^{j-1} \left( ac(T^j)^4 - (I_0^0)^j \right), \quad (3.13a)$$

$$C_v \frac{T^k - T^n}{\Delta t} + \frac{1}{c} \frac{(I_0^0)^k - (I_0^0)^n}{\Delta t} + \frac{\Delta t}{\epsilon} \sum_{j=1}^{k-1} \tilde{a}_{kj} \left( \nabla_{\mathbf{x}} G(I_1^m) \right)^j, \quad (3.13b)$$

$$\frac{\epsilon^2}{c}(I_l^m)^k = \frac{\epsilon^2}{c}(I_l^m)^n - \Delta t \sum_{j=1}^{k-1} \tilde{a}_{kj} \epsilon \left( \nabla_{\mathbf{x}} G(I_{l+1}^m) \right)^j - \Delta t \sum_{j=1}^k a_{kj} \left( \left( \epsilon \nabla_{\mathbf{x}} F(I_{l-1}^m) \right)^j - \sigma^j (I_l^m)^j \right) = 0. \quad (3.13c)$$

*Remark 3.* The coefficients  $I_l^m$  are also numerically solved successively as in (3.10). Since the lower order terms in (3.12c) are already known, the convection terms can be derived explicitly. Moreover, the opacities  $\sigma^l$  in (3.12c) and (3.13c) can be computed explicitly as  $(I_0^0)^{(l)}$  is already known with  $\sigma^0$  chosen as  $\sigma^n$ .

The coefficients  $\tilde{\mathbf{b}} = (\tilde{b}_l)$ ,  $\mathbf{b} = (b_l)$ ,  $\mathcal{A} = (a_{lj})$  and  $\tilde{\mathcal{A}} = (\tilde{a}_{lj})$  can be presented with a double Butcher tableau as

$$\begin{array}{c|c} \tilde{\mathbf{c}} & \tilde{\mathcal{A}} \\ \hline & \tilde{\mathbf{b}}^T \end{array} \quad \begin{array}{c|c} \mathbf{c} & \mathcal{A} \\ \hline & \mathbf{b}^T \end{array} \quad (3.14)$$

The second and third order globally stiffly accurate IMEX schemes used here is the ARS(2, 2, 2) and ARS(4, 4, 3) scheme, where the exact Butcher tableau are as below

$$\begin{array}{c|ccc} 0 & 0 & 0 & 0 \\ \gamma & \gamma & 0 & 0 \\ 1 & \delta & 1-\delta & 0 \\ \hline & \delta & 1-\delta & 0 \end{array} \quad \begin{array}{c|ccc} 0 & 0 & 0 & 0 \\ \gamma & 0 & \gamma & 0 \\ 1 & 0 & 1-\gamma & \gamma \\ \hline & 0 & 1-\gamma & \gamma \end{array}, \quad \gamma = 1 - \frac{1}{\sqrt{2}}, \quad \delta = 1 - \frac{1}{2\gamma}, \quad (3.15)$$

and

$$\begin{array}{c|ccccc} 0 & 0 & 0 & 0 & 0 & 0 \\ 1/2 & 1/2 & 0 & 0 & 0 & 0 \\ 2/3 & 11/18 & 1/18 & 0 & 0 & 0 \\ 1/2 & 5/6 & -5/6 & 1/2 & 0 & 0 \\ 1 & 1/4 & 7/4 & 3/4 & -7/4 & 0 \\ \hline & 1/4 & 7/4 & 3/4 & -7/4 & 0 \end{array} \quad \begin{array}{c|ccccc} 0 & 0 & 0 & 0 & 0 \\ 1/2 & 0 & 1/2 & 0 & 0 & 0 \\ 2/3 & 0 & 1/6 & 1/2 & 0 & 0 \\ 1/2 & 0 & -1/2 & 1/2 & 1/2 & 0 \\ 1 & 0 & 3/2 & -3/2 & 1/2 & 1/2 \\ \hline & 0 & 3/2 & -3/2 & 1/2 & 1/2 \end{array} \quad (3.16)$$

The IMEX RK methods are fully discussed in several literature, and we refer [42, 9, 35] and the references therein for more details.

### 3.3 Fully discrete numerical scheme

We have introduced the time-discretization in the last subsection. In this subsection, the discretization in this spatial space will be discussed. The finite volume method to discretize the spatial space is presented here.

#### 3.3.1 Spatial Discretization

The  $P_N$  equations (2.12) and (2.16) are discretized by finite volume method with linear or third order WENO reconstruction in space. Let  $x_i = i\Delta x$ ,  $z_j = j\Delta z$  and  $t^n = n\Delta t$  be the uniform mesh in Cartesian coordinates. Let  $(i, j)$  denote the cell  $\{(x, z) : x_{i-1/2} < x < x_{i+1/2}, z_{j-1/2} < z < z_{j+1/2}\}$ .  $(I_{i,j,l}^m)^n$  and  $T_{i,j}^n$  are the averaged expansion coefficients of the radiation intensity and the temperature respectively. To get the numerical flux for  $P_N$  system, we rewrite the convection part of (3.10a) and (3.10c) together as

$$\mathcal{C} = \epsilon \left( \bar{\mathbf{A}}_x^{\text{low}} \frac{\partial \bar{\mathbf{I}}}{\partial x} + \bar{\mathbf{A}}_z^{\text{low}} \frac{\partial \bar{\mathbf{I}}}{\partial z} \right)^{n+1} + \epsilon \left( \bar{\mathbf{A}}_x^{\text{up}} \frac{\partial \bar{\mathbf{I}}}{\partial x} + \bar{\mathbf{A}}_z^{\text{up}} \frac{\partial \bar{\mathbf{I}}}{\partial z} \right)^n, \quad (3.17)$$

where  $\bar{\mathbf{A}}_x^{\text{low}}$ ,  $\bar{\mathbf{A}}_z^{\text{low}}$ ,  $\bar{\mathbf{A}}_x^{\text{up}}$ ,  $\bar{\mathbf{A}}_z^{\text{up}}$  are made up by  $F(I_{l-1}^m)$  and  $G(I_{l+1}^m)$  respectively with  $\bar{\mathbf{I}} = (I_0^0, I_1^{-1}, I_1^0, \dots)$ . The Lax-Friedrichs scheme is utilized here to get the numerical flux as

$$\begin{aligned} \left( \epsilon \bar{\mathbf{A}}_x^s \frac{\partial \bar{\mathbf{I}}}{\partial x} \right)_{i,j}^l &\approx \frac{1}{\Delta x} \left( \mathcal{F}_{i,j}^{s,l}(\bar{\mathbf{I}}_{i,j}^l, \bar{\mathbf{I}}_{i+1,j}^l) - \mathcal{F}_{i,j}^{s,l}(\bar{\mathbf{I}}_{i-1,j}^l, \bar{\mathbf{I}}_{i,j}^l) \right), \quad l = n, n+1, \quad s = \text{low, up}, \\ \left( \epsilon \bar{\mathbf{A}}_z^s \frac{\partial \bar{\mathbf{I}}}{\partial z} \right)_{i,j}^l &\approx \frac{1}{\Delta z} \left( \mathcal{G}_{i,j}^{s,l}(\bar{\mathbf{I}}_{i,j}^l, \bar{\mathbf{I}}_{i,j+1}^l) - \mathcal{G}_{i,j}^{s,l}(\bar{\mathbf{I}}_{i,j-1}^l, \bar{\mathbf{I}}_{i,j}^l) \right), \quad l = n, n+1, \quad s = \text{low, up}, \end{aligned} \quad (3.18)$$

where the exact form of  $\mathcal{F}_{i,j}^{s,l}(U_1, U_2)$  and  $\mathcal{G}_{i,j}^{s,l}(U_1, U_2)$  are

$$\mathcal{S}_{i,j}^{s,l}(U_1, U_2) = \frac{\epsilon}{2} \bar{\mathbf{A}}_w^s(U_1 + U_2) + \text{coe}(s, l) \frac{\alpha_{i,j} \epsilon}{2} (U_2 - U_1), \quad w = x, z, \quad \mathcal{S} = \mathcal{F}, \mathcal{G}, \quad s = \text{low, up}, \quad (3.19)$$

with

$$\alpha_{i,j} = \alpha(\sigma_{i,j}, \epsilon) = \exp(-\sigma_{i,j}/\epsilon^2), \quad (3.20)$$

and

$$\text{coe}(s, l) = \begin{cases} 1, & s = \text{up or } (l = M \text{ and } s = \text{low}), \\ 0, & \text{otherwise.} \end{cases} \quad (3.21)$$

The coefficients  $\alpha(\sigma, \epsilon)$  is chosen to ensure the stability of the numerical scheme when  $\epsilon$  is small. The numerical scheme will reduce to the central difference scheme with  $\epsilon$  going to zero. The diffusion term will only appear once in the numerical flux, which will be controlled by the coefficients  $\text{coe}(s, l)$ .

#### 3.3.2 Algorithm

Below we summarize the steps of our numerical scheme.

1. Given  $\bar{\mathbf{I}}_{i,j}^n$  and  $T_{i,j}^n$  at time step  $n$ ;
2. Update the intensity variable and temperature according to the IMEX scheme by using (3.12), (3.13) and (3.18), including the step below at the internal stage  $k$  of a RK step
  - (a) Get  $T_{i,j}^k$  and  $(I_0^0)_{i,j}^k$  by solving the equations (3.13a) and (3.13b);
  - (b) Get  $(I_l^m)_{i,j}^k$  by (3.13c);
3. Goto 1 for the next computational step.

In our computation, the iteration is utilized to make sure the stability of the numerical scheme. The iteration scheme for the semi-discrete first order scheme (3.10) is as below:

$$\begin{aligned} \frac{\epsilon^2}{c} \frac{(I_0^0)^{n+1,s} - (I_0^0)^n}{\Delta t} + \epsilon \left( \nabla_{\mathbf{x}} G(I_1^m) \right)^{n+1,s-1} &= \sigma^{n+1,s-1} \left( ac(T^{n+1,s})^4 - (I_0^0)^{n+1,s} \right), \\ C_v \frac{T^{n+1,s} - T^n}{\Delta t} + \frac{1}{c} \frac{(I_0^0)^{n+1,s} - (I_0^0)^n}{\Delta t} + \frac{1}{\epsilon} \left( \nabla_{\mathbf{x}} G(I_1^m) \right)^{n+1,s-1} &= 0, \\ \frac{\epsilon^2}{c} \frac{(I_l^m)^{n+1,s} - (I_l^m)^n}{\Delta t} + \epsilon \left( \nabla_{\mathbf{x}} F(I_{l-1}^m) \right)^{n+1,s} + \epsilon \left( \nabla_{\mathbf{x}} G(I_{l+1}^m) \right)^{n+1,s-1} &= -\sigma^{n+1,s} (I_l^m)^{n+1,s}, \end{aligned} \quad (3.22)$$

with  $S^{n+1,0} = S^n$  and  $s \in \mathbb{N}$ . The stop criteria is

$$\frac{1}{\Delta t} \left( \|\bar{\mathbf{I}}^{n+1,s+1} - \bar{\mathbf{I}}^{n+1,s}\|_{l_2} + \|T^{n+1,s+1} - T^{n+1,s}\|_{l_2} \right) < \epsilon_0. \quad (3.23)$$

The similar iteration could also be applied to the high order IMEX scheme, and only quite few iterations are needed in the computation.

## 4 Formal asymptotic property and stability analysis

In this section, we will study the asymptotic property and the stability for the proposed AP IMEX scheme.

### 4.1 Formal asymptotic analysis

The asymptotic preserving property is quite important for multi-scale problems. In the realistic thermal radiative transfer problems, it is not practical to resolve the mean-free path, since it requires prohibitively small grid cells. Therefore, the AP property is required for these problems. It is expected that when holding the mesh size and time step fixed, the AP scheme should automatically recover the discrete diffusion solution when the Knudsen number goes to zero [39, 14, 18, 19, 31]. For the radiative transfer problem (2.1), this is to say the numerical method could give a valid discretization of the limiting diffusion equation (2.6) [26].

We will examine the AP property of our method in the asymptotic limit away from boundary and initial layers. Without loss of generality, the first order numerical scheme is studied. In the analysis, the Lax-Friedrichs numerical flux is utilized. The theorem below shows the AP property of this new method.

**Theorem 1.** *As the Knudsen number  $\epsilon$  goes to zero, the numerical scheme proposed in 3.3.2 approaches an explicit five-point scheme for the diffusion limit equation (2.6).*

*Proof.* From (3.5) and (3.10c), it holds that

$$-\sigma^{n+1} (I_1^m)^{n+1} \approx \epsilon \left( \nabla_{\mathbf{x}} F(I_0^m) \right)^{n+1} = \epsilon \left( \frac{\partial}{2\partial x} \left( -C_0^{m-1} I_0^{m-1} + \mathcal{E}_0^{m+1} I_0^{m+1} \right) + \frac{\partial}{\partial z} A_0^m I_0^m \right)^{n+1}, \quad |m| \leq 1. \quad (4.1)$$

With the numerical flux (3.18), we can derive the final approximation to  $(I_1^m)_{i,j}^{n+1}$  at grid  $(i, j)$ . Precisely, the exact expression for  $(I_1^m)_{i,j}^n, m = -1, 0, 1$  is

$$\begin{aligned} (I_1^0)_{i,j}^n &= \frac{-\epsilon}{\sigma_{i,j}^n} \left( \sqrt{\frac{1}{3}} \frac{(I_0^0)_{i,j+1}^n - (I_0^0)_{i,j-1}^n}{\Delta z} + \frac{\alpha_{i,j}^n \epsilon}{2c} \frac{((I_1^0)_{i,j+1}^n - 2(I_1^0)_{i,j}^n + (I_1^0)_{i,j-1}^n)}{\Delta z} \right), \\ (I_1^{-1})_{i,j}^n &= \frac{-\epsilon}{\sigma_{i,j}^n} \left( \sqrt{\frac{2}{3}} \frac{(I_0^0)_{i+1,j}^n - (I_0^0)_{i-1,j}^n}{2\Delta x} + \frac{\alpha_{i,j}^n \epsilon}{2c} \frac{(I_1^{-1})_{i+1,j}^n - 2(I_1^{-1})_{i,j}^n + (I_1^{-1})_{i-1,j}^n}{\Delta x} \right), \\ (I_1^1)_{i,j}^n &= \frac{\epsilon}{\sigma_{i,j}^n} \left( \sqrt{\frac{2}{3}} \frac{(I_0^0)_{i+1,j}^n - (I_0^0)_{i-1,j}^n}{2\Delta x} + \frac{\alpha_{i,j}^n \epsilon}{2c} \frac{(I_1^1)_{i,j}^n - 2(I_1^1)_{i,j}^n + (I_1^1)_{i-1,j}^n}{\Delta x} \right). \end{aligned} \quad (4.2)$$

With the numerical flux (3.18), the fully discretized form of (3.10b) is reduced into

$$C_v \frac{T_{i,j}^{n+1} - T_{i,j}^n}{\Delta t} + \frac{1}{c} \frac{(I_0^0)_{i,j}^{n+1} - (I_0^0)_{i,j}^n}{\Delta t} + \frac{1}{\epsilon} \left( \frac{\mathcal{F}_{i+1/2,j}^n - \mathcal{F}_{i-1/2,j}^n}{\Delta x} + \frac{\mathcal{G}_{i,j+1/2}^n - \mathcal{G}_{i,j-1/2}^n}{\Delta z} \right) = 0, \quad (4.3)$$



where

$$\begin{aligned}\mathcal{F}_{i+1/2,j,g}^n &= \frac{1}{4}\sqrt{\frac{2}{3}}\left(\left((I_1^{-1})_{i,j}^n - (I_1^1)_{i,j}^n\right) + \left((I_1^{-1})_{i+1,j}^n - (I_1^1)_{i+1,j}^n\right)\right) + \frac{\alpha_{i,j}^n \epsilon}{4c}\left((I_0^0)_{i+1,j}^n - (I_0^0)_{i,j}^n\right), \\ \mathcal{G}_{i,j+1/2,g}^n &= \frac{1}{2\sqrt{3}}\left((I_1^0)_{i,j}^n + (I_1^0)_{i,j+1}^n\right) + \frac{\alpha_{i,j}^n \epsilon}{4c}\left((I_0^0)_{i,j+1}^n - (I_0^0)_{i,j}^n\right).\end{aligned}\quad (4.4)$$

From (5.5), we can get that

$$\lim_{\epsilon \rightarrow 0} \alpha_{i,j}^n = \lim_{\epsilon \rightarrow 0} \exp(-\sigma_{i,j}^n / \epsilon^2) = 0. \quad (4.5)$$

Substituting (4.2) into (4.4) and omitting the higher order term of  $\epsilon$ , it holds that

$$\begin{aligned}& \frac{1}{\epsilon} \left( \frac{\mathcal{F}_{i+1/2,j,g}^n - \mathcal{F}_{i-1/2,j,g}^n}{\Delta x} + \frac{\mathcal{G}_{i,j+1/2,g}^n - \mathcal{G}_{i,j-1/2,g}^n}{\Delta z} \right) \\ &= -\frac{1}{3} \left( \frac{\frac{(I_0^0)_{i+2,j}^n - (I_0^0)_{i,j}^n}{2\Delta x \sigma_{i+1,j}^n} - \frac{(I_0^0)_{i,j}^n - (I_0^0)_{i-2,j}^n}{2\Delta x \sigma_{i-1,j}^n}}{2\Delta x} + \frac{\frac{(I_0^0)_{i,j+2}^n - (I_0^0)_{i,j}^n}{2\Delta z \sigma_{i,j+1}^n} - \frac{(I_0^0)_{i,j}^n - (I_0^0)_{i,j-2}^n}{2\Delta z \sigma_{i,j-1}^n}}{2\Delta z} \right).\end{aligned}\quad (4.6)$$

Together with (4.4), and (4.6), we can find that (4.3) becomes a five points scheme for the diffusion limit equation (2.6). This shows that the current scheme for RTE (2.1) is an AP scheme.  $\square$

Though the proof is presented for the first order scheme, it can be extended easily to the high order IMEX RK scheme.

## 4.2 Energy stability

In this section, the general nonlinear stability of the numerical scheme for the complete system and the stability property of the discrete asymptotic limit will be discussed.

### 4.2.1 Gray radiative transfer equation

Just to show the property of the numerical scheme,  $P_N$  equations for gray RTE system in a one-dimensional planar geometry medium is studied. The exact form of the gray radiative transfer equations and the corresponding  $P_N$  equations are presented in Appendix A.1. Without loss of generality, the opacity  $\sigma(x, T)$  and heat capacity  $C_v$  are all treated as constant. The periodic boundary condition is adopted in the spatial space. In this case, the first order scheme (3.10) is reduced into

$$\frac{\epsilon^2}{c} \frac{\bar{\mathbf{I}}_i^{n+1} - \bar{\mathbf{I}}_i^n}{\Delta t} + \Gamma^{\text{low}}(\bar{\mathbf{I}}_i^{n+1}) + \Gamma^{\text{up}}(\bar{\mathbf{I}}_i^n) = -\sigma \bar{\mathbf{I}}_i^{n+1} + ac\sigma (T^4)_i^{n+1} \mathbf{e}_1, \quad (4.7a)$$

$$\epsilon^2 C_v \frac{T_i^{n+1} - T_i^n}{\Delta t} + \frac{\epsilon^2}{c} \frac{I_{0,i}^{n+1} - I_{0,i}^n}{\Delta t} + \Gamma^{\text{up}}(\bar{\mathbf{I}}_i^n) \mathbf{e}_1 = 0. \quad (4.7b)$$

where the numerical flux is defined as

$$\Gamma^s(U_i) = \frac{\mathcal{F}^s(U_{i+1}, U_i) - \mathcal{F}^s(U_i, U_{i-1})}{\Delta x}, \quad s = \text{up, low}, \quad (4.8)$$

with  $\mathcal{F}^s(U_1, U_2)$  defined in (3.19),  $\mathbf{e}_1$  defined in Appendix A.1, and the matrix  $\bar{\mathbf{A}}_x^s$  changed into  $\mathbf{B}^s$  defined in Appendix A.1.

We will begin from the initial gray RTE equation to establish the numerical stability analysis for (4.7). The proposition below shows the energy inequality for gray RTE as,

**Proposition 2.** *For the RTE (A.1) with constant opacity  $\sigma$  and periodic boundary in the spatial space, then the energy inequality holds*

$$\frac{\epsilon^2}{2c} \frac{\partial}{\partial t} \int_{x \in L} \int_{-1}^1 I^2 d\mu dx + \frac{\epsilon^2 C_v}{5} \frac{\partial}{\partial t} \int_{x \in L} \frac{1}{2} ac T^5 dx \leq 0. \quad (4.9)$$

*Proof.* Multiplying (A.1a) with  $I$  and taking integration over  $\mu$  and  $x$ , with the periodic boundary we can derive that

$$\frac{\epsilon^2}{2c} \frac{\partial}{\partial t} \int_{x \in L} \int_{-1}^1 I^2 d\mu dx = \sigma \int_{x \in L} \left( \frac{1}{2} ac T^4 \int_{-1}^1 I d\mu - \int_{-1}^1 I^2 d\mu \right) dx, \quad (4.10)$$

Multiplying (A.1b) with  $\frac{ac}{2}T^4$  and integrating over  $x$ , we can derive that

$$\frac{\epsilon^2 C_v}{5} \frac{\partial}{\partial t} \int_{x \in L} \frac{1}{2} ac T^5 = \sigma \int_{x \in L} \left( \frac{1}{2} ac T^4 \int_{-1}^1 I d\mu - \frac{1}{2} (ac T^4)^2 \right) dx. \quad (4.11)$$

Together with (4.10) and (4.11), it holds with Cauchy-Schwarz inequality that

$$\begin{aligned} & \frac{\epsilon^2}{2c} \frac{\partial}{\partial t} \int_{x \in L} \int_{-1}^1 I^2 d\mu dx + \frac{\epsilon^2 C_v}{5} \frac{\partial}{\partial t} \int_{x \in L} \frac{1}{2} ac T^5 dx \\ &= \sigma \int_{x \in L} \left( ac T^4 \int_{-1}^1 I d\mu - \frac{1}{2} (ac T^4)^2 - \int_{-1}^1 I^2 d\mu \right) dx \\ &\leq \frac{-\sigma}{2} \int_{x \in L} \left( ac T^4 - \int_{-1}^1 I d\mu \right)^2 dx \leq 0. \end{aligned} \quad (4.12)$$

Then we finish the proof of Proposition 2.  $\square$

Based on the energy inequality for the continuous equations, the stability results for the first order scheme (4.7) is listed in the theorem below

**Theorem 2.** *When the Knudsen number  $\epsilon$  is small, the following stability result holds for the first order penalty-based AP scheme defined in (4.7),*

$$\sum_i \left( \frac{\epsilon^2}{2c} \left( \frac{\|\bar{\mathbf{I}}_i^{n+1}\|^2 - \|\bar{\mathbf{I}}_i^n\|^2}{\Delta t} \right) + \epsilon^2 ac C_v \frac{(T_i^5)^{n+1} - (T_i^5)^n}{5\Delta t} \right) \leq 0. \quad (4.13)$$

*Proof.* Similar method will be adopted to get this estimation. First multiplying  $\bar{\mathbf{I}}_i^{n+1}$  on both side of (4.7a), we can derive that

$$\frac{\epsilon^2}{c} \bar{\mathbf{I}}_i^{n+1} \left( \frac{\bar{\mathbf{I}}_i^{n+1} - \bar{\mathbf{I}}_i^n}{\Delta t} \right) + \epsilon \bar{\mathbf{I}}_i^{n+1} \left( \Gamma_i^{\text{low}}(\bar{\mathbf{I}}_i^{n+1}) + \Gamma_i^{\text{up}}(\bar{\mathbf{I}}_i^n) \right) = -\sigma \bar{\mathbf{I}}_i^{n+1} \bar{\mathbf{I}}_i^{n+1} + ac \sigma \bar{\mathbf{I}}_{i,0}^{n+1} (T_i^4)^{n+1} e_1. \quad (4.14)$$

It holds for  $\bar{\mathbf{I}}_i^{n+1}$  that

$$\frac{\epsilon^2}{c} \bar{\mathbf{I}}_i^{n+1} \left( \frac{\bar{\mathbf{I}}_i^{n+1} - \bar{\mathbf{I}}_i^n}{\Delta t} \right) = \frac{\epsilon^2}{2c} \left( \frac{\|\bar{\mathbf{I}}_i^{n+1}\|^2 - \|\bar{\mathbf{I}}_i^n\|^2}{\Delta t} \right) + \frac{\epsilon^2}{2c} \left( \frac{\|\bar{\mathbf{I}}_i^{n+1} - \bar{\mathbf{I}}_i^n\|^2}{\Delta t} \right), \quad (4.15)$$

where  $\|\bar{\mathbf{I}}\|$  is the  $l_2$  norm of the vector  $\bar{\mathbf{I}}$ . Together with (4.7a) and (4.7b), we can derive that

$$\epsilon^2 C_v \frac{T_i^{n+1} - T_i^n}{\Delta t} = -\sigma \left( ac (T_i^4)^{n+1} + I_{i,0}^{n+1} \right). \quad (4.16)$$

Similarly, multiplying  $ac(T_i^4)^{n+1}$  on the both sides of (4.16), we can get that

$$\epsilon^2 C_v (ac T_i^4)^{n+1} \frac{T_i^{n+1} - T_i^n}{\Delta t} = -\sigma (ac T_i^8)^{n+1} + \sigma (ac T_i^4)^{n+1} I_{i,0}^{n+1}. \quad (4.17)$$

Similarly, it holds for  $T_i^4$  that

$$\begin{aligned} \epsilon^2 C_v (ac T_i^4)^{n+1} \frac{T_i^{n+1} - T_i^n}{\Delta t} &= \epsilon^2 ac C_\mu \left( \frac{(T_i^5)^{n+1} - (T_i^5)^n}{5\Delta t} \right. \\ &\quad \left. + \left( (T_i^2)^{n+1} - (T_i^2)^n \right)^2 (4(T_i^3)^{n+1} + 3(T_i^2)^{n+1}(T_i)^n + 2(T_i)^{n+1}(T_i^2)^n + (T_i^3)^n) \right). \end{aligned} \quad (4.18)$$

Together with (4.14), (4.15), (4.17) and (4.18), we can derive the energy estimation for the numerical scheme (4.7) as

$$\sum_i \left( \frac{\epsilon^2}{2c} \left( \frac{\|\bar{\mathbf{I}}_i^{n+1}\|^2 - \|\bar{\mathbf{I}}_i^n\|^2}{\Delta t} \right) + \epsilon^2 ac C_v \frac{(T_i^5)^{n+1} - (T_i^5)^n}{5\Delta t} \right) \leq - \sum_i \left( I_{i,0}^{n+1} - (ac T_i^4)^{n+1} \right)^2 \leq 0. \quad (4.19)$$

Then we can finish the proof.  $\square$

*Remark 4.* The related stability results can be expanded to the high order IMEX RK scheme for the gray radiative transfer equations.

### 4.2.2 The discrete asymptotic limit

In the diffusion limit, the numerical scheme (3.10) will reduce into the forward Euler scheme (4.6). To analyze the behavior of the method in the diffusion limit, the von Neumann analysis on a linear version is applied. In the interest of clarity, we will still focus on the gray problem (A.1) with constant opacity  $\sigma$  and  $C_v$ . In this case, the numerical scheme for the diffusion limit is reduced into

$$C_v \frac{T_i^{n+1} - T_i^n}{\Delta t} + a \frac{(T_i^4)^{n+1} - (T_i^4)^n}{\Delta t} = \frac{ac}{3\sigma} \frac{(T_{i+2}^4)^n - 2(T_i^4)^n + (T_{i-2}^4)^n}{4\Delta x^2}. \quad (4.20)$$

Following the similar method in [26], and focusing on the linear version of (4.20), the final scheme is

$$\frac{\phi_i^{n+1} - \phi_i^n}{\Delta t} = \frac{c}{3\sigma} \frac{\phi_{i+2}^n - 2\phi_i^n + \phi_{i-2}^n}{4\Delta x^2}, \quad \phi_i = T_i^4. \quad (4.21)$$

The solution is decomposed into individual Fourier modes

$$\phi_i^n = \alpha_n \exp(ik\Delta x), \quad (4.22)$$

and (4.21) becomes

$$\frac{\beta_n - 1}{\Delta t} = \frac{c}{3\sigma\Delta x^2} (\cos(2\Delta x) - 1), \quad \beta_n = \frac{\alpha_{n+1}}{\alpha_n}. \quad (4.23)$$

Therefore, the growth rate satisfies

$$\beta_n = 1 + \frac{c\Delta t}{3\sigma\Delta x^2} (\cos(2\Delta x) - 1). \quad (4.24)$$

The stability condition for  $|\beta_n| \leq 1$  is then

$$\frac{c\Delta t}{3\sigma\Delta x^2} \leq \frac{1}{\max |\cos(2\Delta x) - 1|} = 1. \quad (4.25)$$

*Remark 5.* The time step limitation imposed on (4.25) is independent of  $\epsilon$ , which is a gain from time step constraints for the explicit method to solve RTE (2.1) when  $\epsilon$  is small. Moreover, (4.25) is imposed on the diffusion limit. When  $\epsilon$  is not so small, the energy exchange terms are treated implicitly in the numerical scheme, and the only constrain on time step length is the convection term. Thus, we take the time step to satisfy

$$\frac{\Delta t c}{\Delta x} < \text{CFL}. \quad (4.26)$$

## 5 Numerical results

In this section, several numerical simulations for the radiative transfer equations in spatially 1D and 2D cases are studied to check the performance of our methods. We have implemented the first order (3.10) and third order IMEX RK scheme (3.12) to approximate RTE. In all the 1D numerical tests, the CFL number is set as  $\text{CFL} = 0.4$ . For 2D test cases, the CFL number is set as  $\text{CFL} = 0.1$ . Periodic and inflow boundary conditions are implemented, the details of which is presented in (A.2).

### 5.1 The AP property

This example is designed to test the AP property and the order of accuracy of our new methods for the first order scheme (3.10). The test starts with an equilibrium initial data

$$T = (3 + \sin(\pi x))/4, \quad I = acT^4, \quad x \in L. \quad (5.1)$$

The computation region is  $L = [0, 2]$  with the periodic boundary condition imposed on both ends. The parameters are set as  $a = c = 1.0$ ,  $C_v = 0.1$  and  $\sigma = 10$ . Similar tests can be found in the literature for the Boltzmann equation [43].

In this test, the mesh size is  $N = 100$  and the expansion order of the  $P_N$  method is  $M = 7$ . Since we are going to test the behavior of the numerical scheme when  $\epsilon$  goes to zero, the time step is set as  $\Delta t = \text{CFL}\Delta x^2/c$ . Figure 1a shows the time evolution of the error  $\mathcal{E}_{\text{AP}}$  as

$$\mathcal{E}_{\text{AP}} = \sum_{i=1}^N \left( (I_{0,i} - T_i)^2 + \sum_{j=1}^M I_{j,i}^2 \right), \quad (5.2)$$

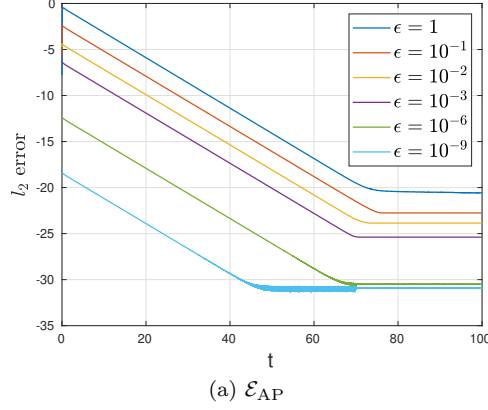


Figure 1: Time evolution of  $\mathcal{E}_{AP}$  with different  $\epsilon$ .

for the numerical scheme (3.10) for different  $\epsilon$ , from which we can see that for any  $\epsilon$ , the error is decreasing with time and then reaches a final steady state. With the decreasing of  $\epsilon$ , the final error gets smaller, which shows the AP property of the numerical scheme.

Next, we test the order of the numerical scheme (3.10). The initial data (5.1) with the same parameters are applied. We compute the solutions with grid size  $N = 50, 100, 200, 400$  and  $800$  respectively for  $\epsilon = 1, 0.1$  and  $0.01$ . The final time is  $t = 0.5$ , and the numerical solution with  $N_0 = 1600$  is chosen as the reference solution. The  $l_2$  error between the numerical solution and the reference solution with different  $\epsilon$  are calculated. Figure 2 shows the convergence order of the numerical method for different  $\epsilon$ . It shows that for different  $\epsilon$ , the scheme is first order uniformly which also validates the AP property of the numerical scheme.

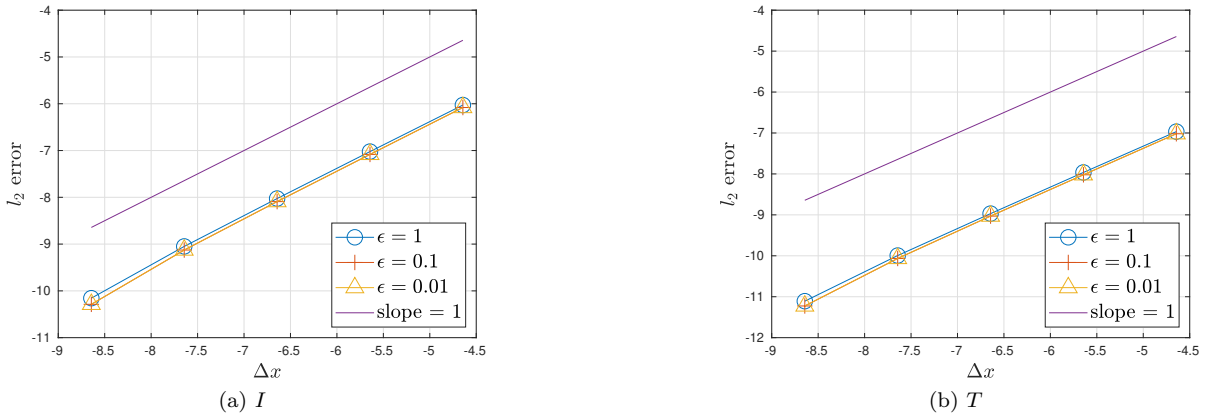


Figure 2:  $l_2$  error between the numerical solution with grid size as  $N = 50, 100, 200, 400$  and  $800$  and the reference solution, where the reference solution is the numerical solution with  $N = 1600$ . (a) the  $l_2$  error of the radiation intensity  $I$ . (b) the  $l_2$  error of the material temperature  $T$ .

## 5.2 Marshak wave problems

In the following examples, the classical Marshak wave problems are tested. The Marshak problem is one of the benchmark problems and is also studied in several literature such as [39, 20, 26]. In our computations, the parameters are chosen the same as that in [39] with  $a = 0.01372 \text{ GJ/cm}^3 - \text{keV}^4$  and  $c = 29.98 \text{ cm/ns}$ . In this section, two absorption/emission coefficients are tested.

**Marshak Wave-2B** In this example, we take the absorption/emission coefficient to be  $\sigma = 100/T^3 \text{ cm}^2/\text{g}$ , the density is  $3.0 \text{ g/cm}^3$  and the specific heat to be  $0.1 \text{ GJ/g/keV}$ . The initial material temperature  $T$  is set to be  $10^{-6} \text{ keV}$ . A constant isotropic incident radiation intensity with a Planckian distribution at  $1 \text{ keV}$  is kept on the left boundary. The computation region is  $[0, \infty)$  but taken to be  $L = [0, 0.2]$  in our

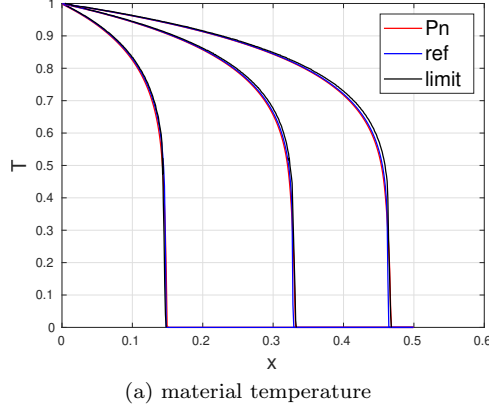


Figure 3: The material temperature  $T$  of Marshak 2B problem at time  $t = 10, 50$  and  $100$ , where the red line is the numerical solution to RTE, the blue line is the reference solution and the black line is that to diffusive limit.

simulations. In this case,  $\sigma$  is large enough that the solution to RTE is almost the same as the diffusive limit results.

In the test, the expansion order of  $P_N$  is set as  $M = 11$  with the grid size  $N = 400$ . The third order IMEX RK scheme (3.12) is applied here, where the time step is chosen as  $\Delta t = \text{CFL} \Delta x / c$ . In Figure 3, the numerical results of the radiation wave front at time 10, 50 and 100 are plotted. The reference solution is from [26] and the diffusive limit result is get by the finite difference method. From Figure 3, we can find that the numerical solution to RTE is on top of each other with that of the reference solution and the diffusive limit results, which is also consistent with our expectation that the solution to RTE is almost the same as the diffusive limit.

**Marshak Wave-2A** Marshak-2A problem is quite similar to Marshak-2B problem, except that its absorption/emission coefficient is  $\sigma = 10/T^3 \text{cm}^2/\text{g}$ . For this case, since  $\sigma$  is not large enough, the solution to RTE is different from that of the diffusion limit.

In this test, the same numerical setting as Marshak wave B is chosen. In Figure 4a, the computed radiation wave front at time  $t = 0.2, 0.4, 0.6, 0.8$  and  $1.0$  are given. Figure 4b presents the computed material temperature for both gray radiation transfer equations and diffusion limiting equation at time  $t = 1$ , where the reference solution is from [16]. From it, we can see that the numerical solution matches the reference solution well, but is quite different from the diffusive limit.

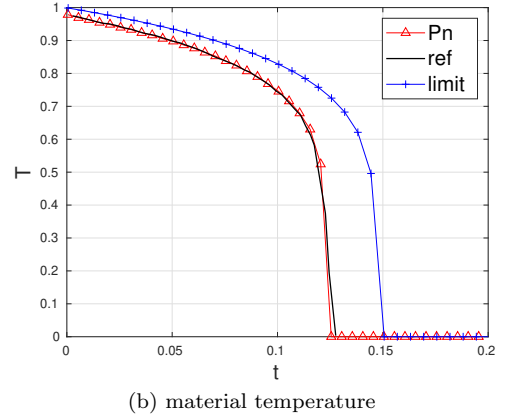
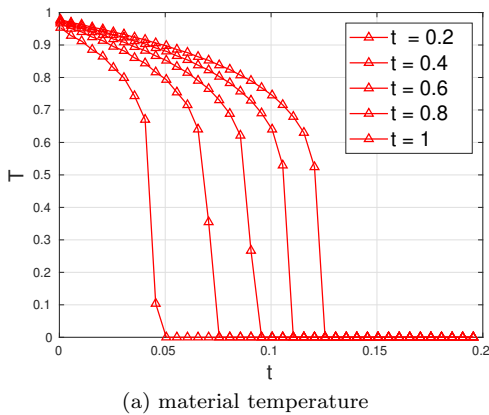


Figure 4: The material temperature  $T$  of Marshak 2A problem at different time. (a) The material temperature  $T$  of Marshak 2A problem at  $t = 0.2, 0.4, 0.6, 0.8$  and  $1$ . (b) The material temperature  $T$  of Marshak 2A problem at  $t = 1$ , where the red line is the numerical solution to RTE, the black line is the reference solution and the blue line is that to diffusive limit.

From the numerical results of Marshak wave problems, we can find that the new numerical scheme

works well both for the optical thick and thin problems. The time step length is independent from the absorption coefficients  $\sigma$ , which shows the high efficiency of this AP numerical scheme.

### 5.3 A lattice problem

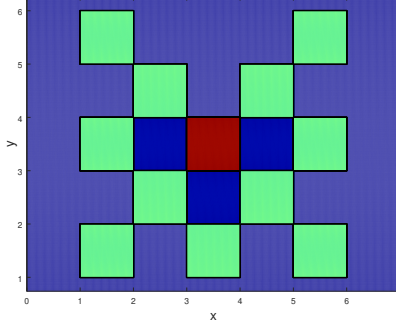


Figure 5: Layout of the lattice problem.

In this section, we study a two-dimensional problem with the added complication of multiple materials but without radiation-material coupling. We consider the transfer equation

$$\frac{\epsilon^2}{c} \frac{\partial I}{\partial t} + \epsilon \mathbf{\Omega} \cdot \nabla I = -\sigma_a I + \sigma_s \left( \frac{1}{4\pi} \int_{\mathbb{S}^2} I d\mathbf{\Omega} - I \right) + \epsilon^2 G. \quad (5.3)$$

Photons are absorbed with a power density of  $\frac{c\sigma_a}{\epsilon^2} I$ . As there is no radiation-material coupling, the photons are simply removed from the system when the absorption occurs. The isotropic scattering term does not change the radiation temperature but causes the specific intensity  $I$  to become more evenly distributed in microscopic velocity. The computation domain is  $[0, 7] \times [0, 7]$ . It consists of a set of squares belonging to a strongly absorbing medium in a background of weakly scattering medium. The specific layout of the problem is given in Figure 5, where the blue regions and the dark red region are purely scattering medium with  $\sigma_s = 1$  and  $\sigma_a = 0$ ; the light green regions contain purely absorbing material with  $\sigma_s = 0$  and  $\sigma_a = 10$ . In the dark red region, there is an isotropic source  $G = \frac{1}{4\pi}$ , and  $G$  is zero elsewhere. Initially the specific intensity is at equilibrium and the radiation temperature is  $10^{-6}$ . Vacuum boundary conditions are imposed on all four sides of the computation domain, which means there is an outflow of radiation but no inflow. Other parameters are set as  $c = a = \epsilon = 1$ .

We use a mesh of  $280 \times 280$  in the spatial space and  $P_5$  is adopted here. Moreover, the filtering technique is applied in the microscopic velocity space to avoid negative energy density solution. Filtering techniques as proposed in [30] are employed in 2D simulations to suppress spurious oscillations in  $P_N$  solutions. The filtering applied here is only applied to  $l \geq 2M/3$ , where  $M$  is the highest order of spherical harmonic expansion [8, 5]. For these  $l$ , before the updating of each time step, we substitute  $I_l^m$  with  $\hat{I}_l^m$ , which satisfy

$$\hat{I}_l^m = \frac{I_l^m}{1 + \alpha l^2 (l+1)^2}, \quad (5.4)$$

where

$$\alpha = \frac{\omega}{M^2} \frac{1}{[(\sigma_a + \sigma_s)L + M]^2}, \quad \omega = \frac{2c\Delta t}{\Delta x}. \quad (5.5)$$

with  $L$  the characteristic length of the problem, which is taken to be  $L = 1$  for all our simulations.  $\sigma_a$  and  $\sigma_s$  are the absorption and scattering coefficients, respectively.

In the test, the first order scheme (3.10) is used for temporal discretization and a third order WENO reconstruction is used in spatial discretization. The results at time  $t = 3.2$  are summarized in Figure 6 with the logarithm of density distribution to the base 10 shown in contour and slice. In Figure 6, our solutions are compared with the solution by StaRMAP [37] as reproduced from [36]. Even though we use different space and time discretization method from [37], both solutions agree with each other quite well. Both are able to produce the beams of particles leaking between the corners of the absorbing regions. Moreover, at the end time, the wave front should have just propagated to the domain boundary, a property satisfied by our simulation results.

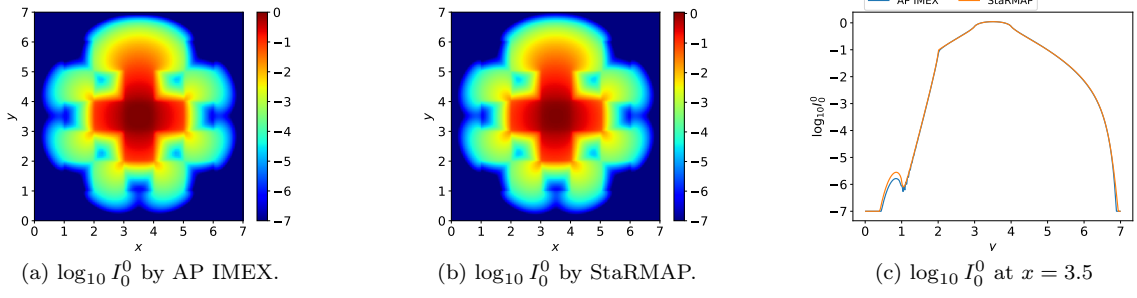


Figure 6: The contour and slice plot of  $\log_{10} I_0^0$  for the lattice problem at  $t = 3.2$ . (a) Contour plot of our solution. (b) The contour plot of the solution reproduced using StaRMAP. (c) Comparison between our solution and that reproduced from StaRMAP at  $x = 3.5$ .

#### 5.4 A hohlraum problem

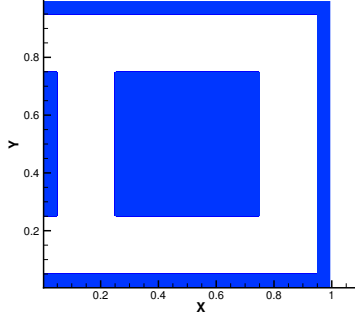


Figure 7: Layout of the hohlraum problem. The blue region is where  $(x, y) \in [0, 0.05] \times [0.25, 0.75]$ , and  $(x, y) \in [0.25, 0.75] \times [0.25, 0.75]$ ,  $(x, y) \in [0, 1] \times [0, 0.05]$ ,  $(x, y) \in [0, 1] \times [0.95, 1]$  and  $(x, y) \in [0.95, 1] \times [0, 1]$ .

This section studies a hohlraum problem similar to that studied in [30]. For this problem, radiation field is coupled to the material energy. It is well known that the diffusion approximation fails to capture the correct physics of this type of problem [1, 30], making it necessary to simulate the original RTE which has the form (2.1). Also, in this problem, the material is initially cold and optically thick, and then becomes optically thinner as radiation heats it up. The wide range in optical depth presents a challenge to numerical schemes. The layout of the problem is shown in Figure 7. The computation domain is  $[0, 1] \times [0, 1]$ , in which the white areas are vacuum with  $\sigma_a = 0$ . The blue regions in Figure 7 satisfy  $\sigma_a = 100/T^3 \text{ cm}^2/\text{g}$ , while the density is  $1.0 \text{ g/cm}^3$  and the heat capacity  $C_v$  is  $0.3 \text{ GJ/g/keV}$ . An isotropic inflow of 1 keV black body source is incident on the entire left boundary. In our computation, we take  $\epsilon = 1$ ,  $a = 0.01372 \text{ GJ/cm}^3 - \text{keV}^4$  and  $c = 29.98 \text{ cm/ns}$ . We use a  $100 \times 100$  mesh in physical space and a  $P_N$  method with  $M = 7$ . The same filtering techniques as in the last section is applied here. As with the previous example, the first order scheme is used for time discretization and a third order WENO reconstruction is used in spatial discretization.

Figure 8 and 9 compare the contour plots of our solution for the radiation temperature and the material temperature at  $t = 1$  with the implicit Monte Carlo solution taken from [30]. The radiation temperature is defined as

$$T_{\text{rad}} = \sqrt[4]{\frac{I_0^0}{ac}}. \quad (5.6)$$

We can find that they agree well with each other, which validates our new numerical scheme. Same as the IMC solution, our solution permits the photons to bend around the front wall, and at the end time of our simulation, the back wall is just starting to heat up and re-emit photons. It was pointed out in [30] that the solution to this problem has the following two properties, the first one is non-uniform heating of the central block, and the other is less radiation directly behind the block than those regions

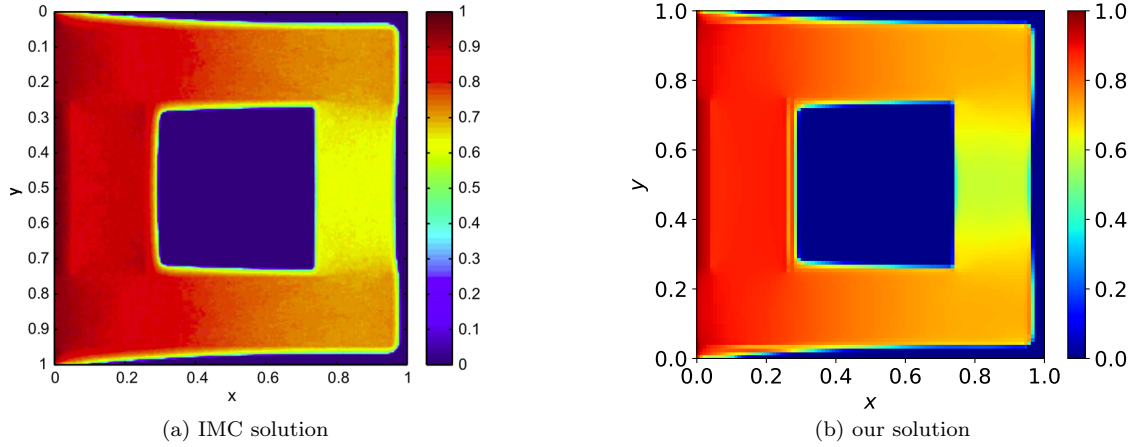


Figure 8: The contour plots of radiation temperature of the hohlraum problem at  $t = 1$ . (a) The IMC solution taken from [30]. (b) Our solution.

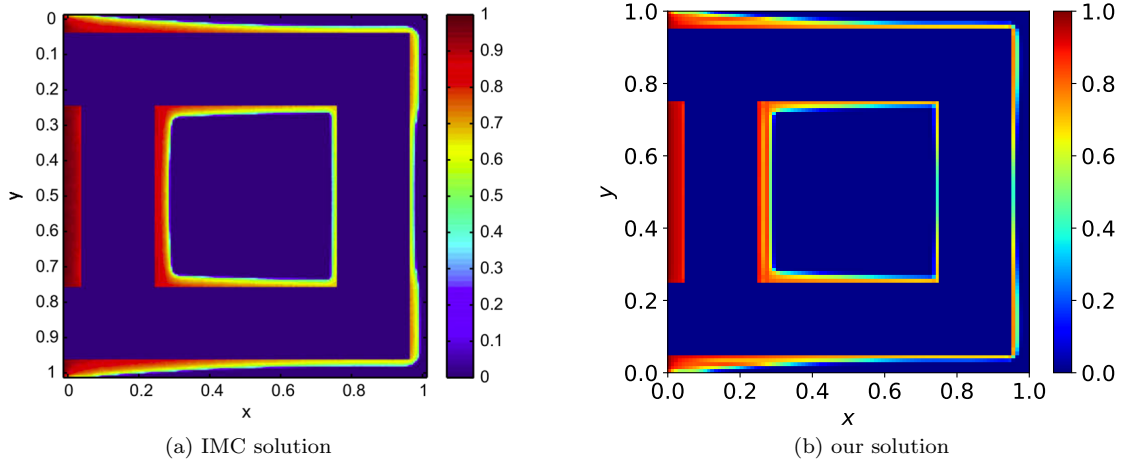


Figure 9: The contour plots of material temperature of the hohlraum problem at  $t = 1$ . (a) The IMC solution taken from [30]. (b) Our solution.

within the line of sight of the source. The numerical results show that our solution satisfies both these properties, which also verifies the effect of our numerical scheme. Following [30], we plot the solutions along  $y = 0.125$  and  $x = 0.85$  in Figure 10. In both figures, our solutions are in rough agreement with the IMC solution, which is considered the benchmark for this test case.

## 6 Conclusions

In this paper, we have developed an AP IMEX numerical scheme for the RTE system in the framework of  $P_N$  method. The Maxwellian iteration is utilized to derive the order of each expansion coefficients of the radiation intensity based on Knudsen number. Thus, in each equation of  $P_N$  system, the term at lower order of Knudsen is set as implicit term with those at higher order of Knudsen set as explicit term. Therefore, the implicit-explicit  $P_N$  system can be solved at the computational cost of a completely explicit scheme with the time step length proportional to the mesh size and independent on Knudsen number. The analysis of the total energy shows the energy stability with the evolution of time. Numerical examples have exhibited the AP property and the efficiency of this new scheme. However, this method is limited to the gray model for the moment. Research works on the multi-frequency problem are ongoing.



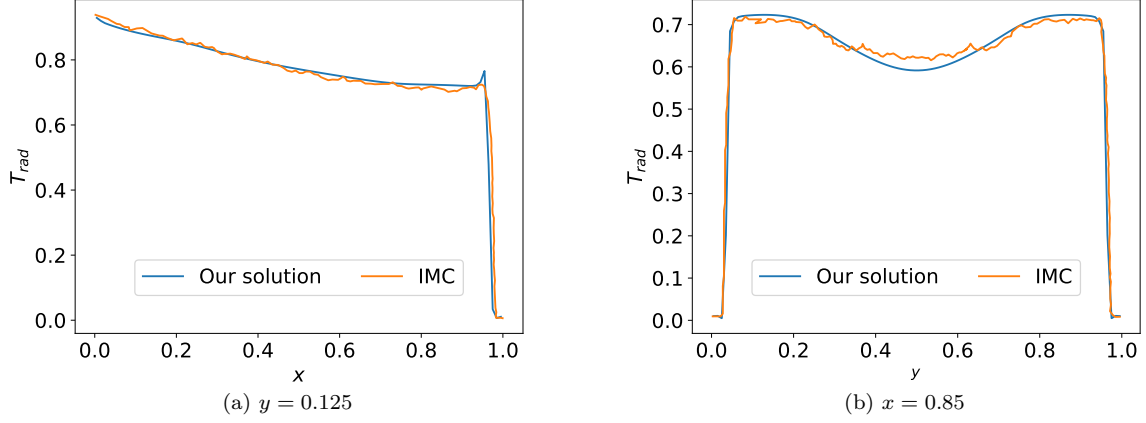


Figure 10: Comparison of the radiation temperature of the hohlraum problem computed by IMC method and our method at  $t = 1$  on different slices. (a) Comparison at  $y = 0.125$ . (b) Comparison at  $x = 0.85$ .

## Acknowledgements

We thank Prof. Ruo Li from PKU, Prof. Zhenning Cai from NUS, Prof. Tao Xiong from XMU and Prof. Jiequan Li, Prof. Wenjun Sun, Dr. Yi Shi from IAPCM for their valuable suggestions. Weiming Li is partially supported by the Science Challenge Project (No. TZ2016002). Peng Song is partially supported by the Science Challenge Project (No. TZ2016002), the CAEP foundation (No. CX20200026) and the National Natural Science Foundation of China (Grant No. 91630310). The work of Yanli Wang is partially supported by Science Challenge Project (No. TZ2016002) and the National Natural Science Foundation of China (Grant No. U1930402).

## A Appendix

### A.1 Gray model of the radiative transfer equations for 1D angle problem and related $P_N$ equations

The time-dependent gray radiative transfer [26] in a one-dimensional planar geometry medium has the form as

$$\frac{\epsilon^2}{c} \frac{\partial I}{\partial t} + \epsilon \mu \frac{\partial I}{\partial x} = \sigma \left( \frac{1}{2} acT^4 - I \right), \quad x \in [0, L], \quad (\text{A.1a})$$

$$\epsilon^2 C_v \frac{\partial T}{\partial t} = \sigma \left( \int_{-1}^1 I d\mu - acT^4 \right), \quad (\text{A.1b})$$

where  $I(t, \mu, x)$  is the intensity of radiation,  $\mu = \cos \theta \in [-1, 1]$  is the internal coordinate associated with the angle  $\theta \in [0, \pi]$ .  $T(t, x)$  is the material temperature, and  $\sigma$  is the absorption opacity.

For (A.1), the basis function for the  $P_N$  method is the Legendre polynomials. The moments are defined as

$$I_l = \int_{-1}^1 P_l(\mu) I(t, x, \mu) d\mu, \quad l = 0, \dots, M, \quad (\text{A.2})$$

where  $P_l$  is the Legendre polynomial. Then the  $P_N$  equations for (A.1) is

$$\begin{aligned} \frac{\epsilon^2}{c} \frac{\partial \bar{\mathbf{I}}}{\partial t} + \epsilon \mathbf{B}^{\text{low}} \frac{\partial \bar{\mathbf{I}}}{\partial x} + \epsilon \mathbf{B}^{\text{up}} \frac{\partial \bar{\mathbf{I}}}{\partial x} &= -\sigma \bar{\mathbf{I}} + \sigma acT^4 \mathbf{e}_1, \\ \epsilon^2 C_v \frac{\partial T}{\partial t} &= \sigma (I_0 - acT^4), \end{aligned} \quad (\text{A.3})$$

where  $\bar{\mathbf{I}} = (I_0, I_1, \dots, I_M)$  and  $\mathbf{e}_1 = (1, 0, \dots, 0)^T$ .  $\mathbf{B}^{\text{low}}$  and  $\mathbf{B}^{\text{up}}$  are triangular matrix with the non-zero entries as

$$\mathbf{B}^{\text{low}}(i+1, i) = \frac{i-1}{2(i-1)+1}, \quad \mathbf{B}^{\text{up}}(i, i+1) = \frac{i}{2(i-1)+1}, \quad i = 1, \dots, M. \quad (\text{A.4})$$

## A.2 Inflow boundary condition for $P_N$ equations

We implement the inflow boundary condition for the  $P_N$  equations by specifying the values of coefficients of the  $P_N$  system in ghost cells. We first discuss how the inflow boundary condition is implemented in 1D spatial case. Choose the left boundary as an example. The incoming radiation intensity incident on the boundary interface is

$$I(\mu) = I^b(\mu), \quad \text{for } \mu > 0. \quad (\text{A.5})$$

For the  $P_N$  method, the numerical boundary can be rewritten as

$$I^{\text{ghost}}(\mu) = \begin{cases} I^b(\mu), & \mu > 0 \\ I^i(\mu), & \mu < 0, \end{cases} \quad (\text{A.6})$$

where  $I^i(\mu)$  is the radiation intensity at the left boundary of the area. Then the expansion coefficients at the ghost cell is

$$I_l^{\text{ghost}} = \int_{-1}^1 I^{\text{ghost}}(\mu) P_l(\mu) d\mu. \quad (\text{A.7})$$

The implementation of the inflow boundary condition in 2D is similar in spirit to that of 1D. Denote by  $\mathbf{n}$  the outward normal of the boundary interface. The incident radiation intensity on the boundary is

$$I(\mathbf{\Omega}) = I^b(\mathbf{\Omega}), \quad \text{for } \mathbf{\Omega} \cdot \mathbf{n} < 0. \quad (\text{A.8})$$

For the  $P_N$  method, the numerical boundary can be rewritten as

$$I^{\text{ghost}}(\mathbf{\Omega}) = \begin{cases} I^b(\mathbf{\Omega}), & \mathbf{\Omega} \cdot \mathbf{n} < 0, \\ I^i(\mathbf{\Omega}), & \mathbf{\Omega} \cdot \mathbf{n} > 0, \end{cases} \quad (\text{A.9})$$

where  $I^i(\mathbf{\Omega})$  is the radiation intensity on the interior side of the boundary interface we consider. Then the expansion coefficients at the ghost cell is

$$\begin{aligned} I_l^{m,\text{ghost}} &= \int_{\mathbb{S}^2} I^{\text{ghost}}(\mathbf{\Omega}) \overline{Y_l^m}(\mathbf{\Omega}) d\mathbf{\Omega} \\ &= \int_{\mathbf{\Omega} \cdot \mathbf{n} < 0} I^b(\mathbf{\Omega}) \overline{Y_l^m}(\mathbf{\Omega}) d\mathbf{\Omega} + \int_{\mathbf{\Omega} \cdot \mathbf{n} > 0} I^i(\mathbf{\Omega}) \overline{Y_l^m}(\mathbf{\Omega}) d\mathbf{\Omega} \\ &= \int_{\mathbf{\Omega} \cdot \mathbf{n} < 0} I^b(\mathbf{\Omega}) \overline{Y_l^m}(\mathbf{\Omega}) d\mathbf{\Omega} + \sum_{j=0}^M \sum_{k=-j}^j I_j^{k,i} \int_{\mathbf{\Omega} \cdot \mathbf{n} > 0} Y_j^k(\mathbf{\Omega}) \overline{Y_l^m}(\mathbf{\Omega}) d\mathbf{\Omega} \end{aligned} \quad (\text{A.10})$$

The integrations  $\int_{\mathbf{\Omega} \cdot \mathbf{n} > 0} Y_j^k(\mathbf{\Omega}) \overline{Y_l^m}(\mathbf{\Omega}) d\mathbf{\Omega}$  do not depend on the solutions, and are computed and stored before the beginning of each simulation.

## References

- [1] T. A. Brunner. Forms of approximate radiation transport. *Sandia report*, 2002.
- [2] Z. Cai and R. Li. Numerical regularized moment method of arbitrary order for Boltzmann-BGK equation. *SIAM J. Sci. Comput.*, 32(5):2875–2907, 2010.
- [3] J. Densmore. Asymptotic analysis of the spatial discretization of radiation absorption and re-emission in Implicit Monte Carlo. *J. Comput. Phys.*, 230(4):1116–1133, 2011.
- [4] J. Densmore, H. Park, A. Wollaber, R. Rauenzahn, and D. Knoll. Monte Carlo simulation methods in moment-based scale-bridging algorithms for thermal radiative-transfer problems. *J. Comput. Phys.*, 284:40–58, 2015.
- [5] Y. Di, Y. Fan, Z. Kou, R. Li, and Y. Wang. Filtered hyperbolic moment method for the vlasov equation. *J. Sci. Comput.*, 79(2):969–991, 2019.
- [6] J. Fleck and J. Cummings. An implicit Monte Carlo scheme for calculating time and frequency dependent nonlinear radiation transport. *J. Comput. Phys.*, 8(3):313–342, 1971.

- [7] N. Gentile. Implicit Monte Carlo diffusionan acceleration method for Monte Carlo time-dependent radiative transfer simulations. *J. Comput. Phys.*, 172(2):543–571, 2001.
- [8] T. Hou and R. Li. Computing nearly singular solutions using pseudo-spectral methods. *J. Comput. Phys.*, 226(1):379–397, 2007.
- [9] J. Jang, F. Li, J. Qiu, and T. Xiong. High order asymptotic preserving DG-IMEX schemes for discrete-velocity kinetic equations in a diffusive scaling. *J. Comput. Phys.*, 281:199–224, 2015.
- [10] S. Jin and C. Levermore. The discrete-ordinate method in diffusive regimes. *Transp. Theory Stat. Phys*, 20(1-2):413–439, 1991.
- [11] S. Jin and C. Levermore. Fully discrete numerical transfer in diffusive regimes. *Transp. Theory Stat. Phys*, 22(6):739–791, 1993.
- [12] S. Jin, L. Pareschi, and G. Toscani. Uniformly accurate diffusive relaxation schemes for multiscale transport equations. *SIAM J. Numer. Anal.*, 38(3):913–936, 2000.
- [13] D. Kershaw. Flux limiting natures own way. *Technical Report UCRL-78378, Lawrence Livermore National Laboratory, Livermore, CA*, 1976.
- [14] A. Klar. An asymptotic-induced scheme for nonstationary transport equations in the diffusive limit. *SIAM J. Numer. Anal*, 35(6):1073–1094, 1998.
- [15] R. Koch, W. Krebs, S. Wittig, and R. Viskanta. Discrete ordinates quadrature schemes for multi-dimensional radiative transfer. *J. Quant. Spectrosc. Ra.*, 53(4):353–372, 1995.
- [16] Los Alamos National Laboratory. An implicit Monte Carlo code for thermal radiative transfer: Capabilities, development, and usag. *LA-14195-MS*, 2000.
- [17] V. Laboure, R. McClarren, and C. Hauck. Implicit filtered  $P_N$  for high-energy density thermal radiation transport using discontinuous galerkin finite elements. *J. Comput. Phys.*, 321:624–643, 2016.
- [18] A. Larsen and J. Morel. Asymptotic solutions of numerical transport problems in optically thick, diffusive regimes. *J. Comput. Phys.*, 69(2):283–324, 1987.
- [19] A. Larsen and J. Morel. Asymptotic solutions of numerical transport problems in optically thick, diffusive regimes. ii. *J. Comput. Phys.*, 83(1):212–236, 1989.
- [20] E. Larsen, A. Kumar, and J. Morel. Properties of the implicitly time-differenced equations of thermal radiation transport. *J. Comput. Phys.*, 238:82–96, 2013.
- [21] K. Lathrop and B. Garlson. Discrete ordinates angular quadrature of the neutron transport equation. *Los Alamos Scientific Laboratory*, 1965.
- [22] E. Lewis and W. Miller. *Computational Methods in Neutron Transport*. United States, 1993.
- [23] W. Li, C. Liu, Y. Zhu, J. Zhang, and K. Xu. A unified gas-kinetic particle method for multiscale photon transport. *arXiv preprint arXiv:1810.05984*, 2018.
- [24] W. Li, C. Liu, Y. Zhu, J. Zhang, and K. Xu. Unified gas-kinetic wave-particle methods iii: Multiscale photon transport. *J. Comput. Phys.*, 408:109280, 2020.
- [25] K. Mathews. On the propagation of rays in discrete ordinates. *Nucl. Sci. Eng.*, 132:155–180, 1999.
- [26] R. McClarren, T. Evans, R. Lowrie, and J. Densmore. Semi-implicit time integration for pn thermal radiative transfer. *J. Comput. Phys.*, 227(16):7561–7586, 2008.
- [27] R. McClarren and C. Hauck. Robust and accurate filtered spherical harmonics expansions for radiative transfer. *J. Comput. Phys.*, 229(16):5597–5614, 2010.
- [28] R. McClarren and C. Hauck. Simulating radiative transfer with filtered spherical harmonics. *Phys. Lett. A*, 374(22):2290–2296, 2010.

- [29] R. McClarren, J. Holloway, and T. Brunner. On solutions to the  $P_n$  equations for thermal radiative transfer. *J. Comput. Phys.*, 227(5):2864–2885, 2008.
- [30] R. G. McClarren and C. D. Hauck. Robust and accurate filtered spherical harmonics expansions for radiative transfer. *J. Comput. Phys.*, 229(16):5597–5614, 2010.
- [31] L. Mieussens. On the asymptotic preserving property of the unified gas kinetic scheme for the diffusion limit of linear kinetic models. *Journal of Computational Physics*, 253:138–156, 2013.
- [32] J. Morel, T. Wareing, R. Lowrie, and D. Parsons. Analysis of ray-effect mitigation techniques. *Nucl. Sci. Eng.*, 144:1–22, 2003.
- [33] G. Olson. Second-order time evolution of  $P_N$  equations for radiation transport. *J. Comput. Phys.*, 228(8):3072–3083, 2009.
- [34] H. Park, D. Knoll, R. Rauenzahn, A. Wollaber, and J. Densmore. A consistent, moment-based, multiscale solution approach for thermal radiative transfer problems. *Transp. Theory Stat. Phys.*, 41(3-4):284–303, 2012.
- [35] Z. Peng, Y. Cheng, J. Qiu, and F. Li. Stability-enhanced AP IMEX-LDG schemes for linear kinetic transport equations under a diffusive scaling. *J. Comput. Phys.*, 415:109485, 2020.
- [36] B. Seibold and M. Frank. Starmap code. website.<http://www.math.temple.edu/~seibold/research/starmap>.
- [37] B. Seibold and M. Frank. Starmap-a second order staggered grid method for spherical harmonics moment equations of radiative transfer. *ACM T. Math. Software (TOMS)*, 41(1):4, 2014.
- [38] Y. Shi, P. Song, and W. Sun. An asymptotic preserving unified gas kinetic particle method for radiative transfer equations. *J. Comput. Phys.*, 420:109687, 2020.
- [39] W. Sun, S. Jiang, and K. Xu. An asymptotic preserving unified gas kinetic scheme for gray radiative transfer equations. *J. Comput. Phys.*, 285(15):265–279, 2015.
- [40] W. Sun, S. Jiang, and K. Xu. An asymptotic preserving implicit unified gas kinetic scheme for frequency-dependent radiative transfer equations. *Int. J. Numer. Anal. Mod.*, 15(1-2):134–153, 2018.
- [41] J. Warsa, T. Wareing, and J. Morel. Krylov iterative methods and the degraded effectiveness of diffusion synthetic acceleration for multidimensional  $S_N$  calculations in problems with material discontinuities. *Nucl. Sci. Eng.*, 147:218–248, 2004.
- [42] T. Xiong, J. Jang, F. Li, and J. Qiu. High order asymptotic preserving nodal discontinuous Galerkin IMEX schemes for the BGK equation. *J. Comput. Phys.*, 284:70–94, 2015.
- [43] B. Yan and S. Jin. A successive penalty-based asymptotic-preserving scheme for kinetic equations. *SIAM J. Sci. Comput.*, 35(1):A150–A172, 2013.